Applied Physics A (2023) 129:795
https://doi.org/10.1007/s00339-023-07055-5

Applied Physics A
Materials Science & Processing

Study of time-resolved photoluminescence decay curves in Al-doped ZnO and Eu-doped $Cd_{1-x}Zn_xS$ nanophosphors

Monika Monica[1] · Reena Reena[1] · Sukhjeet Singh[2] · Suhaas Gupta[3] · Stuti Tomar[4] · Ravi Kant Choubey[5] · S. Gaurav[5] · Tejendra K. Gupta[6] · Dimple Kumari[7] · Sunil Kumar[8]

Received: 10 August 2023 / Accepted: 4 October 2023

Abstract
Even though the excited state lifetimes can be found out experimentally using well-known time-resolved spectroscopy but low signal to noise ratio leading to lack of data points on the hyperbolic curves makes it difficult to clearly reproduce the individual exponentials simply by fitting to further analyse the decay curves. Keeping these things in mind, in this work, time-resolved photoluminescent emission decay curves were simulated for aluminium doped zinc oxide [ZnO:Al (0.1–3.0%)] nanophosphors and europium doped cadmium-zinc sulphide [$Cd_{1-x}Zn_xS$:Eu (0.01–10.00%, $x = 0$–0.5)] nanocomposite phosphor using FORTRAN-77 subroutines for three different lifetimes. Excited state lifetime is the most important parameter of nanophosphors to investigate for the purpose of opto-electronic applications, among emission intensity and wavelength. Experimentally obtained excited state lifetimes were used as the primary input to study the effect of various parameters like cut-off intensity, dopant concentration and nanocomposite composition on the decay nature of emission intensities from individual excited states, and the decay nature of total emission intensity. Decay curves generated for the ZnO:Al (0.1–3.0%) nanophosphors displayed the lifetime shortening and enhanced emission due to increasing Al-doping at all simulated arbitrary intensities for all excited state lifetimes. Decay curves generated for the $Cd_{1-x}Zn_xS$:Eu (0.01–10.00%, $x = 0$–0.5) nanocomposite phosphors similarly displayed the trend of lifetime shortening with increasing Zn-concentration and Eu-doping for every individually simulated exponential.

Keywords Time-resolved spectroscopy · Photoluminescence · Decay curve · Nanophosphor

1 Introduction

Phosphors are luminescent materials that convert absorbed energy into visible-light emissions at room temperature, unlike incandescent materials that exhibit light emission only at high temperatures. Phosphors are primarily

Monika Monica and Reena Reena Contributed equally as a first author.

✉ Sunil Kumar
sunil.physics@igu.ac.in

[1] Department of Physics, Maharishi Markandeshwar University, Mullana, Ambala 133207, Haryana, India

[2] Department of Physics, Akal University, Talwandi Sabo 151302, Punjab, India

[3] Department of Condensed Matter Physics, Faculty of Mathematics and Physics, Charles University, Ke Karlovu 5, 12116 Prague, Czech Republic

[4] Applied Science and Humanities Department, ABES Engineering College, Campus-1, 19Th KM Stone, NH-24, Ghaziabad 201009, Uttar Pradesh, India

[5] Department of Physics, Amity Institute of Applied Sciences (AIAS), Amity University, Noida Campus, Sector-125, Noida 201313, Uttar Pradesh, India

[6] Department of Chemistry, Amity Institute of Applied Sciences (AIAS), Amity University, Noida Campus, Sector-125, Noida 201313, Uttar Pradesh, India

[7] Department of Chemistry, College of Commerce, Arts and Science, Patna 800020, Bihar, India

[8] Department of Physics, Indira Gandhi University, Meerpur, Rewari 122502, Haryana, India

employed in different capacities in a variety of display devices, including but not limited to cathode ray tube displays, plasma display panels, electro-luminescence-based displays like LED displays, field emission displays, etc. Phosphors also find use in several other applications such as radiation conversion, fluorescent tracing or pigmentation, and other miscellaneous uses as a light source. Confining the phosphorescent material in one (or more) dimension(s) to the nano-size regime (< 100 nm) gives rise to the material class known as nanophosphors, which exhibit markedly improved opto-electronic properties as compared to their bulk counterpart. These enhanced opto-electronic properties of nanophosphors open avenues of application-based research in a variety of fields such as: detection, identification, labelling, and imaging of biomolecules; targeted drug delivery and therapy; photocatalysis; energy storage and conversion; building, filling, and coating of nanocomposite assemblies, etc. [1–9].

At a crystalline structure level, nanomaterials and their bulk counterparts are similar. The origin of modified opto-electronic properties of nanomaterials lies in the quantization of the energy levels due to the strong spatial confinement of their particles, and the subsequent increase in the surface-to-volume ratio of the atoms in the nanomaterial. In semiconductors specifically, when the size of the semiconducting material is comparable to its Bohr excitonic radius, its opto-electronic properties become size dependent. The size of the forbidden energy band gap, and related properties like absorption edge and excitonic emission peak can be tailored by controlling the size of the semiconducting nanomaterial. Surface defects become more pronounced in the nano-size regime due to the large surface-to-volume ratio, and these surface defects act as active energy traps in the forbidden energy band gap, facilitating optical transitions in the material beyond just the valence-to-conduction-band excitonic transition [10–15]. Quantum confinement effects also produce an enhancement in the oscillator strength of nanomaterials, which in turn produces lifetime shortening and enhances the radiative recombination rate; this allows for the use of nanomaterials in the realisation of more efficient and sensitive devices [16–20].

Zinc oxide (ZnO) has a large band gap (~ 3.3 eV), high conductivity, work function and transparency, and exhibits good thermal and mechanical stability when doped. These properties make ZnO an ideal candidate for application as a transparent conductive oxide (TCO) film to be used in extensive opto-electronic devices such as photovoltaic cells, liquid crystal displays, etc. ZnO is particularly a superior replacement to widely used TCO indium tin(-doped) oxide (ITO) because it is more abundant, cheaper, environment-friendly, easier to grow at lower temperatures and etch. ZnO has been doped with a variety of Group A elements that act as n-type dopants, and aluminium (Al^{3+}) doping is the most efficient at lowering the electrical resistivity of ZnO, and creating cationic defect trapping levels [21–25].

Cadmium sulphide (CdS) is a well-known and extensively studied II–VI compound semiconductor whose size-tuneable nanomaterial properties have found various applications in opto-electronic and electronic technology. CdS is highly responsive to visible-light, has a direct band gap of 2.4 eV, and exhibits superior photocatalytic activity among other semiconductor nanomaterials. However, CdS also exhibits fast recombination of photo-generated charge carriers which leads to poor quantum efficiency. This is resolved by coupling the CdS with zinc sulphide (ZnS) in a nanocomposite and by doping with europium (Eu^{3+}), which facilitate collection and separation of charge carriers and their radiative transitions, respectively [26–30]. Nano-sized ZnS is one of the most interesting and commonly investigated II–VI compound semiconductor due to its direct and wide forbidden energy band gap (~ 3.6 eV for cubic zinc-blende phase at room temperature) that can be easily tuned by tailoring the size of the ZnS nanoparticle or with the help of controlled amount of dopant ions. This makes ZnS nanomaterials an extremely popular candidate in a wide-range of applications and devices, most notably as an opto-electronically superior and more environment-friendly alternative to cadmium sulphide (CdS) in photovoltaic cells. Due to its wide-band gap ZnS is most useful within the blue-light region of the electromagnetic spectrum, with limited applications at long wavelengths. This is resolved with the help of suitable dopants, which not only enhance the efficiency of optical transitions, but also increase the number of luminescent centres, inducing tuneable optical emission even at longer wavelengths. Doping with rare-earth elements lends to the nanomaterial narrow emission bands with high quantum efficiencies, as a result of the transitions from within the internal 4f electronic shell [31–35].

When investigating nanophosphors, optical parameters of excited state lifetime, emission wavelength and intensity, decay constant, etc. are extremely important for application-based research. These properties, which are influenced by the optical transitions in the material, can be investigated with nanosecond time-resolved spectroscopy techniques, employing excitation by short and intense laser pulses to detect transient phenomenon [36–38]. However, in some cases, signal to noise ratio is a problem specially in hyperbolic decays for determining deciding factor for the distribution of trap states in the phosphors. Therefore, keeping in mind this problem, in the present work, time-resolved emission decay curves

were simulated for ZnO:Al (0.1–3.0%) and $Cd_{1-x}Zn_xS$:Eu (0.01–10.00%, $x = 0$–0.5) using FORTRAN-77 subroutine executed over microsecond-steps. Primary inputs used include arbitrary values of radiation intensity at cut-off position, and experimental values of excited state lifetimes obtained from previously conducted laser-induced photoluminescent investigations [39, 40], which were recorded using nitrogen (N_2) laser having excitation wavelength of 337.1 nm and pulse width of 5–7 ns operating with an average power of 10 kW and peak power of 1 MW as the excitation source. Solid-state nanophosphors were pasted onto a Perspex sample holder placed at an angle of 45° to the incident laser beam. A fast photomultiplier tube was used to collect the phosphorescent signal from the sample at an angle of 90° to the incident laser beam, through an optical assembly of a wavelength selective monochromator and an UV radiation filtering glass slab, and a digital storage oscilloscope recorded the multi-exponential decay curves.

2 Theory of luminescence

Intensity of phosphorescent radiation (I) at a given time (t) is given by the relation

$$I = I_0.e^{-pt}$$

where I_0 is the radiation intensity at the cut-off position, and p is Einstein's spontaneous coefficient which describes the transition probability of the radiative decay from the excited state. A graph plotted between log$I$ on the y axis and t on the x axis will be a straight line representing a single lifetime of transition. However, in most realistic cases of interactions between radiation and solids, multiple lifetime components are observed in the non-linear graph of log I vs. t that arise due to trapping levels at various depths in the energy band gap. The transition probabilities (P) for the decay from the various traps are obtained from the following relation

$$P = S.e^{\frac{-E}{kT}}$$

where S is the escape frequency factor ($= 10^9\ s^{-1}$), E is the energy of the trapping level in the forbidden energy band gap of the semiconductor (trap-depth), k is the Boltzmann constant, and T is the absolute temperature. Trapping levels at different trap-depths give rise to the multi-exponential decay curve of real laser induced photoluminescence. In an ideal case, there would be an equal number of trapping levels at all depths, i.e., a uniform distribution of trapping levels. However, in most realistic cases the distribution of trapping levels is not uniform, and is instead given by the relation

$$I = I_0.t^{-b}$$

where, b is the deciding factor for the distribution of trap states, also called the decay constant.

FORTRAN-77 subroutine was developed to generate decay curves, where arbitrary values of radiation intensity at cut-off position and transition probabilities were used as the primary inputs. The subroutine was executed over values of t in microsecond-steps, using experimental excited state lifetimes obtained from pulsed laser induced photoluminescence studies conducted previously, where a nitrogen laser having excitation wavelength of 337.1 nm and pulse width of 5–7 ns operating with an average power of 10 kW and peak power of 1 MW was used to excite the short-lived shallow trapping states.

$Cd_{1-x}Zn_xS$:Eu (0.01–10.00%, $x = 0$–0.5) nanophosphors were synthesised using the well-known bottom-up chemical co-precipitation method, and cubic zinc-blende phase was confirmed for all samples at all compositions using powder X-ray diffraction (P-XRD), with Scherrer analysis of broad and highest intensity characteristic (111) peak revealing an average crystallite size of ~ 4 nm. Transverse electron microscope (TEM) image also indicated an average particle size of ~ 4 nm, confirming the strong size confinement (particle size less than Bohr exciton radius) of all the synthesised samples (Supplementary Information, Figures S–S3). Under excitation by 337.1 nm N_2-laser, the $Cd_{1-x}Zn_xS$:Eu (0.01–10.00%, $x = 0$–0.5) nanophosphors exhibited host lattice related violet emission at ~ 430 nm, and Eu-ion related red emission at ~ 617 nm, and this emission was studied in the laser-induced time-resolved analysis [39]. Eu-doping facilitates two separate radiative transitions, red colour $^5D_0 \rightarrow {}^7F_2$, which is dependent on the environment and hence increased in intensity with increased Eu-doping concentration, and orange colour (~ 590 nm) $^5D_0 \rightarrow {}^7F_1$ [32, 33]; in the case of synthesised $Cd_{1-x}Zn_xS$:Eu (0.01–10.00%, $x = 0$–0.5) nanophosphors, the latter orange colour emission was very feeble in comparison to the red colour emission, and hence was not studied in the laser-induced time-resolved analysis. Eu-doping fills up the sulphur vacancies in the host lattice, hence quenching the native defect mediated radiative recombination of electron and holes [31, 34, 35]. Increased Eu-doping also shortened the excitation lifetime of the nanophosphor due to the faster relaxation mechanism facilitated by the dopant energy levels, while increased Zn-concentration promoted the energy transfer from the host to the Eu-centers and thereby also contributed to the lifetime shortening [39].

ZnO:Al (0.1–3.0%) nanophosphors were synthesised using a wet chemical method, and high degree of hexagonal wurtzite crystallinity at all concentrations of Al-doping was confirmed using P-XRD, with Scherrer analysis revealing an average crystallite size of ~ 20 nm. TEM image also indicated an average particle size of 20 nm, with multimode shape and size distribution of the synthesised ZnO:Al (0.1–3.0%) nanoparticles (Supplementary Information, Figures S4–S6) [40]. ZnO nanophosphors typically exhibit excitonic UV emission at ~ 380 nm (which is blue-shifted with decreasing size and increasing energy band gap of the ZnO nanophosphor), and native defect mediated two-center radiative recombination generated green emission at ~ 510 nm. The characteristic green emission is blue-shifted in the case of nanophosphors with decreasing sizes due to increasing concentration of oxygen vacancy related defects which trap holes to recombine with delocalised electrons at the surface [24, 25]. In the case of synthesised ZnO:Al (0.1–3.0%) nanophosphors, however, the green emission is quenched in favour of the Al-ion photoluminescent center mediated intense blue emission at ~ 440 nm, which increased in intensity with increasing Al-doping concentration, and this emission was studied in the laser-induced time-resolved analysis. Along with the strong chemical affinity of aluminium and oxygen decreasing the amount of oxygen related defects, the increased amount of Al-doping concentration promoted the non-radiative energy transfer to Al-ion photoluminescent centers, which were closer to the ZnO band edges in the forbidden energy band gap. This energy transfer is faster and greatly preferred compared to the hole-trapping and recombination mechanism mediated by the oxygen vacancies, hence inhibiting the spontaneous green emission through native defects of the ZnO nanophosphor [21, 23]. Increased Al-doping also shortened the excitation lifetime of the nanophosphor due to the faster relaxation mechanism facilitated by the dopant energy levels [40].

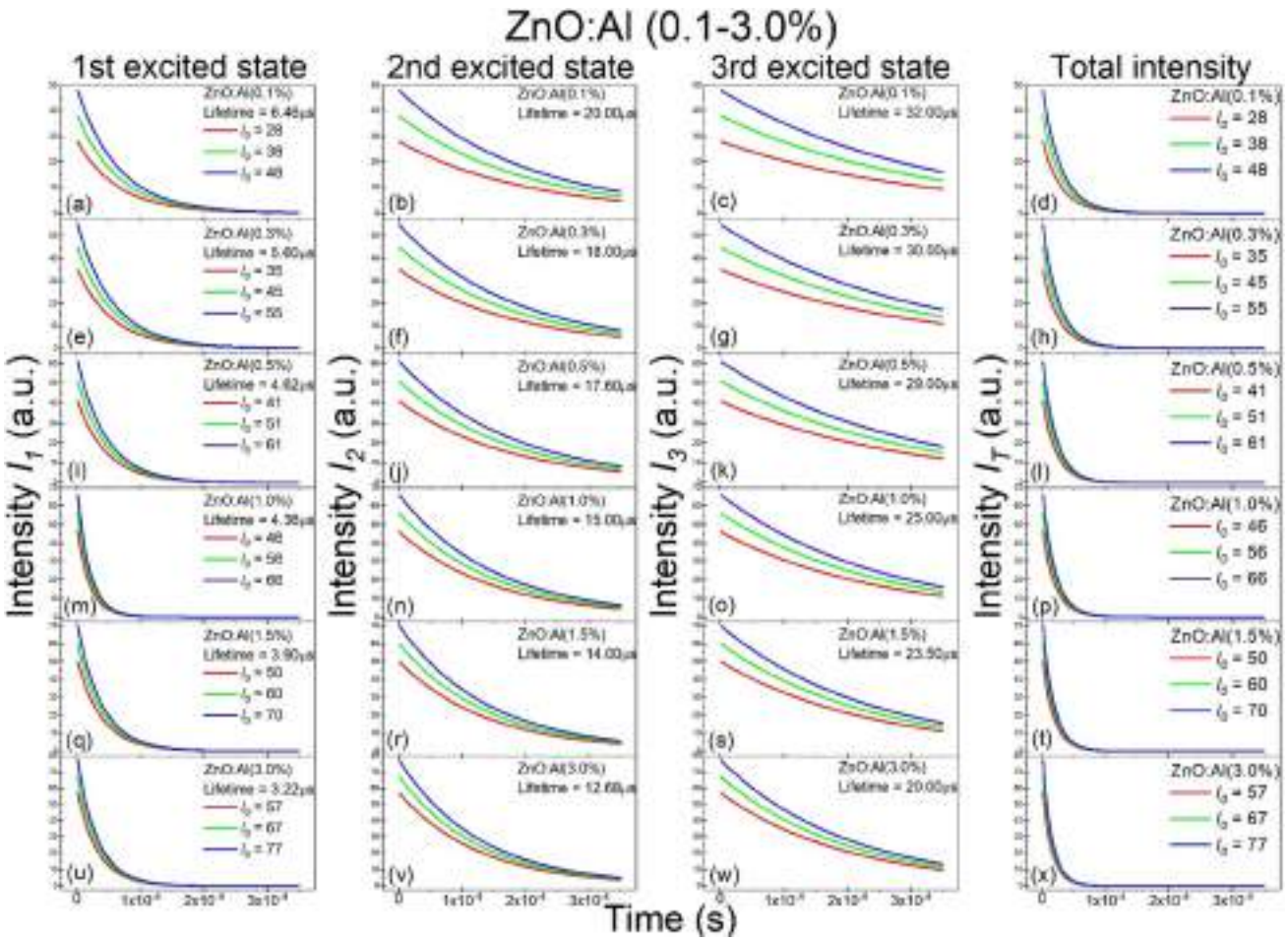

Fig. 1 Simulated time-resolved emission intensity decay curves of ZnO:Al (0.1–3.0%) nanophosphors

3 Generation of decay curves

Figure 1 shows the decay curves generated for ZnO:Al (0.1–3.0%) nanophosphor, with arbitrary cut-off intensity values for every individual excited state lifetime. Figure 1a–d shows four plots of decaying emission intensity with increasing time, where the first three plots (I_1, I_2 and I_3, or Fig. 1a–c, respectively) are decay curves of the individual excited states (exhibiting experimental lifetimes of 6.46 µs, 20.00 µs and 32.00 µs, respectively) and the fourth plot (I_T, Fig. 1d) is the decay curve of the total intensity. In the case of ZnO:Al(0.3%) (Fig. 1e–h), the arbitrary cut-off intensity values are 35, 45 and 55, and the individual excited state lifetimes are 5.60 µs, 18.00 µs and 30.00 µs for I_1, I_2 and I_3, respectively. In the case of ZnO:Al(0.5%) (Fig. 1i–l), the arbitrary cut-off intensity values are 41, 51 and 61, and the individual excited state lifetimes are 4.62 µs, 17.60 µs and 29.00 µs for I_1, I_2 and I_3, respectively. In the case of ZnO:Al(1.0%) (Fig. 1m–p), the arbitrary cut-off intensity values are 46, 56 and 66, and the individual excited state lifetimes are 4.36 µs, 15.00 µs and 25.00 µs for I_1, I_2 and I_3, respectively. In the case of ZnO:Al(1.5%) (Fig. 1q–t), the arbitrary cut-off intensity values are 50, 60 and 70, and the individual excited state lifetimes are 3.90 µs, 14.00 µs and 23.50 µs for I_1, I_2 and I_3, respectively. In the case of ZnO:Al(3.0%) (Fig. 1u–x), the arbitrary cut-off intensity values are 57, 67 and 77, and the individual excited state lifetimes are 3.22 µs, 12.68 µs and 20.00 µs for I_1, I_2 and I_3, respectively. Table 1 summarises the individual excited state lifetimes of the studied ZnO:Al (0.1–3.0%) nanophosphors for different arbitrary cut-off intensity values. Increasing Al-doping shortens the excitation lifetime of the nanophosphor due to the faster relaxation mechanism facilitated by the dopant energy levels. This trend is clearly reproduced in all simulated arbitrary cut-off intensity for every excited state lifetime exponential.

Figures 2, 3, 4, 5 show the decay curves generated for $Cd_{1-x}Zn_xS$:Eu (0.01–10.00%, $x = 0$–0.5) nanophosphors, where the arbitrary cut-off intensity values were the same for all simulations, namely 10, 20 and 30. In the case of CdS:Eu(0.01%) (Fig. 2a–d), the individual excited state lifetimes are 0.52 µs, 1.10 µs and 2.85 µs for I_1, I_2 and I_3, respectively. In the case of CdS:Eu(0.10%) (Fig. 2e–h), the individual excited state lifetimes are 0.50 µs, 1.03 µs and 2.67 µs for I_1, I_2 and I_3, respectively. In the case of CdS:Eu(1.00%) (Fig. 2i–l), the individual excited state lifetimes are 0.49 µs, 0.99 µs and 2.33 µs for I_1, I_2 and I_3, respectively. In the case of CdS:Eu(10.00%) (Fig. 2m–p), the individual excited state lifetimes are 0.47 µs, 0.93 µs and 2.01 µs for I_1, I_2 and I_3, respectively. In the case of $Cd_{0.9}Zn_{0.1}S$:Eu(0.01%) (Fig. 3a–d), the individual excited state lifetimes are 0.51 µs, 1.08 µs and 2.79 µs for I_1, I_2 and I_3, respectively. In the case of $Cd_{0.9}Zn_{0.1}S$:Eu(0.10%) (Fig. 3e–h), the individual excited state lifetimes are 0.49 µs, 0.98 µs and 2.37 µs for I_1, I_2 and I_3, respectively. In the case of $Cd_{0.9}Zn_{0.1}S$:Eu(1.00%) (Fig. 3i–l), the individual excited state lifetimes are 0.46 µs, 0.90 µs and 1.95 µs for I_1, I_2 and I_3, respectively. In the case of $Cd_{0.9}Zn_{0.1}S$:Eu(10.00%) (Fig. 3m–p), the individual excited state lifetimes are 0.42 µs, 0.87 µs and 1.83 µs for I_1, I_2 and I_3, respectively. In the case of $Cd_{0.7}Zn_{0.3}S$:Eu(0.01%) (Fig. 4a–d), the individual excited state lifetimes are 0.37 µs, 0.75 µs and 1.62 µs for I_1, I_2 and I_3, respectively. In the case of $Cd_{0.7}Zn_{0.3}S$:Eu(0.10%) (Fig. 4e–h), the individual excited state lifetimes are 0.34 µs, 0.69 µs and 1.39 µs for I_1, I_2 and I_3, respectively. In the case of $Cd_{0.7}Zn_{0.3}S$:Eu(1.00%) (Fig. 4i–l), the individual excited state lifetimes are 0.29 µs, 0.61 µs and 1.24 µs for I_1, I_2 and I_3, respectively. In the case of $Cd_{0.7}Zn_{0.3}S$:Eu(10.00%) (Fig. 4m–p), the individual excited state lifetimes are 0.24 µs, 0.51 µs and 1.15 µs for I_1, I_2 and I_3, respectively. In the case of $Cd_{0.5}Zn_{0.5}S$:Eu(0.01%) (Fig. 5a–d), the individual excited state lifetimes are 0.18 µs, 0.38 µs and 1.02 µs for I_1, I_2 and I_3, respectively. In the case of $Cd_{0.5}Zn_{0.5}S$:Eu(0.10%) (Fig. 5(e–h)), the individual excited state lifetimes are 0.14 µs, 0.30 µs and 0.93 µs for I_1, I_2 and I_3, respectively. In the case of $Cd_{0.5}Zn_{0.5}S$:Eu(1.00%) (Fig. 5i–l), the individual excited state lifetimes are 0.10 µs, 0.21 µs and 0.63 µs for I_1, I_2 and I_3, respectively. In the case of $Cd_{0.5}Zn_{0.5}S$:Eu(10.00%) (Fig. 5m–p), the individual

Table 1 Individual excited state lifetimes of the studied ZnO:Al (0.1–3.0%) nanophosphors for different arbitrary cut-off intensity values

SAMPLE	Arbitrary cut-off intensity values			Excited state lifetimes (µs)		
	I_0	I_0'	I_0''	τ_1 (I_1)	τ_2 (I_2)	τ_3 (I_3)
ZnO:Al (0.1%)	28	38	48	6.46	20	32
ZnO:Al (0.3%)	35	45	55	5.6	18	30
ZnO:Al (0.5%)	41	51	61	4.62	17.6	29
ZnO:Al (1.0%)	46	56	66	4.36	15	25
ZnO:Al (1.5%)	50	60	70	3.9	14	23.5
ZnO:Al (3.0%)	57	57	77	3.22	12.68	20

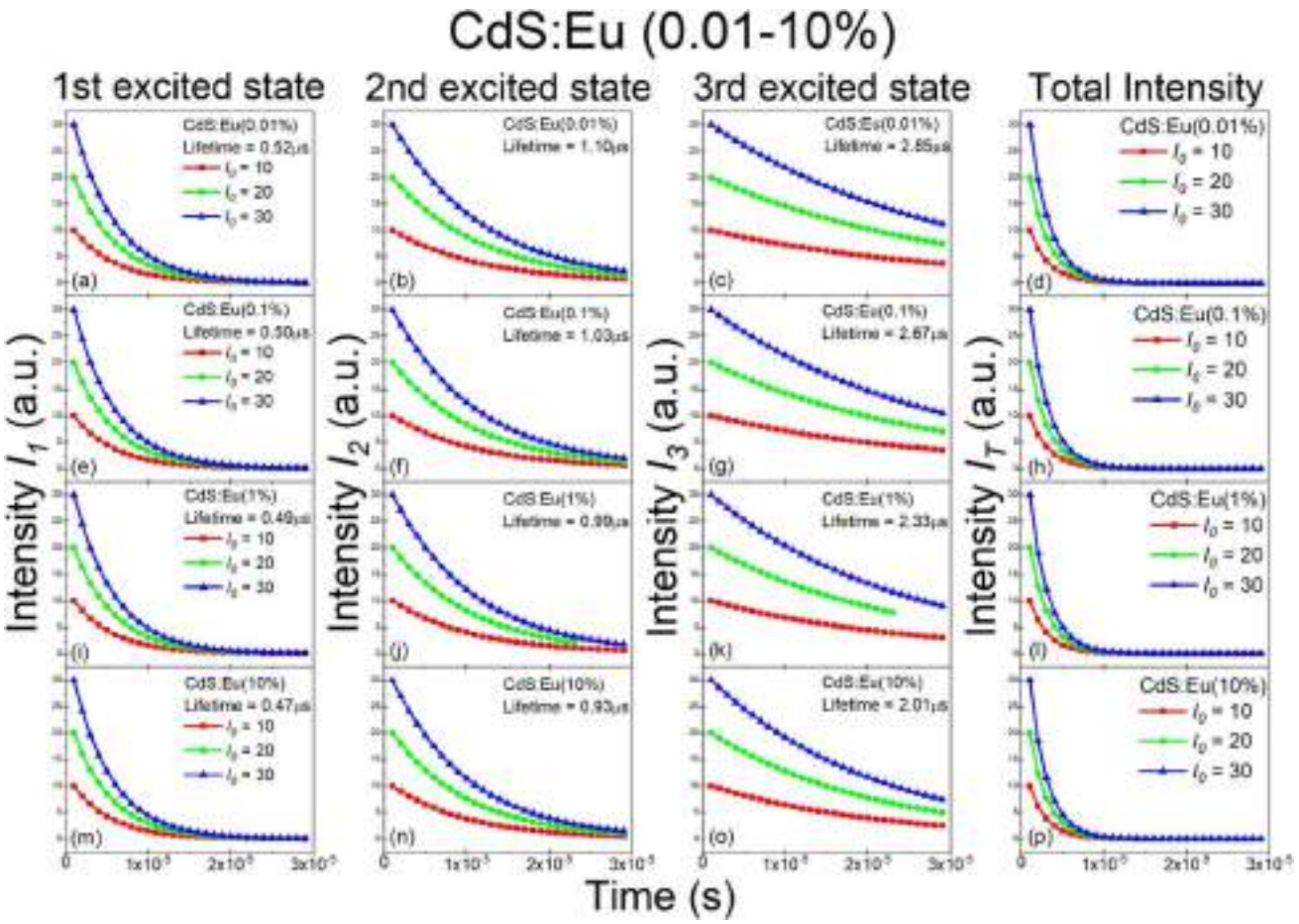

Fig. 2 Simulated time-resolved emission intensity decay curves of CdS:Eu (0.01–10.00%) nanophosphors

excited state lifetimes are 0.05 µs, 0.13 µs and 0.41 µs for I_1, I_2 and I_3, respectively. Table 2 summarises the individual excited state lifetimes of the studied $Cd_{1-x}Zn_xS$:Eu (0.01–10.00%, $x = 0$–0.5) nanophosphors for arbitrary cut-off intensity values of 10, 20 and 30. Increasing Eu-doping shortens the excitation lifetime of the nanophosphor due to the faster relaxation mechanism facilitated by the dopant energy levels, while increasing Zn-concentration promotes energy transfer from the host to the Eu-centers and thereby also contributes to lifetime shortening. These trends are clearly reproduced in all simulated arbitrary cut-off intensity for every excited state lifetime exponential.

4 Results and conclusion

Time-resolved emission decay curves were simulated for ZnO:Al (0.1–3.0%) and $Cd_{1-x}Zn_xS$:Eu (0.01–10.00%, $x = 0$–0.5) using FORTRAN-77 subroutine executed over microsecond-steps; arbitrary values of radiation intensity at cut-off position and experimentally obtained transition probabilities were used as the primary inputs. Experimental excited state lifetimes were obtained from pulsed laser induced photoluminescence studies conducted previously, where a nitrogen laser having excitation wavelength of 337.1 nm and pulse width of 5–7 ns operating with an average power of 10 kW and peak power of 1 MW was used to excite the short-lived shallow trapping states. When investigating the viability of a nanophosphor for optoelectronic applications, emission intensity and wavelength are important characterizations, but the most important parameter is the excited state lifetime. Enhancement of emission and lifetime shortening due to Al doping indicates that ZnO nanoparticles absorb energy and transfer it non-radiatively to Al photoluminescent centers, which is faster than the electron–hole recombination mechanism behind the emission of native ZnO. Recorded results show lifetime shortening for emissions with increasing concentration of Zn, due to

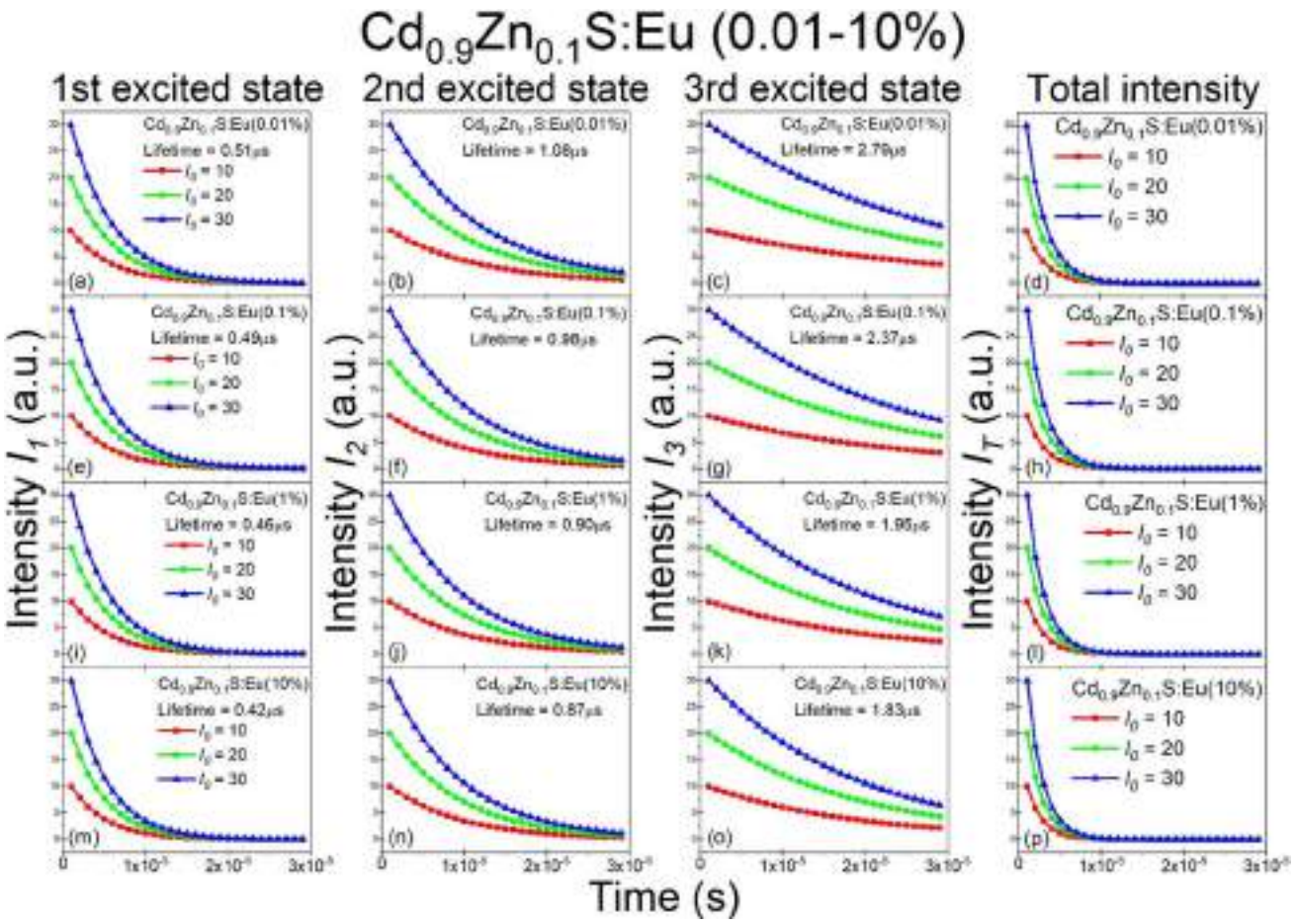

Fig. 3 Simulated time-resolved emission intensity decay curve of $Cd_{0.9}Zn_{0.1}S$:Eu (0.01–10.00%) nanocomposite phosphors

Table 2 Individual excited state lifetimes of the studied $Cd_{1-x}Zn_xS$:Eu (0.01–10.00%, $x = 0$–0.5) nanophosphors for arbitrary cut-off intensity values of 10, 20 and 30

Excited state lifetimes (μs)	CdS:Eu				$Cd_{0.9}Zn_{0.1}S$:Eu			
	0.01%	0.10%	1.00%	10.00%	0.01%	0.10%	1.00%	10.00%
τ_1 (I_1)	0.52	0.5	0.49	0.47	0.51	0.49	0.46	0.42
τ_2 (I_2)	1.1	1.03	0.99	0.93	1.08	0.98	0.9	0.87
τ_3 (I_3)	2.85	2.67	2.33	2.01	2.79	2.37	1.96	1.83
Excited state lifetimes (μs)	$Cd_{0.7}Zn_{0.3}S$:Eu				$Cd_{0.5}Zn_{0.5}S$:Eu			
	0.01%	0.10%	1.00%	10.00%	0.01%	0.10%	1.00%	10.00%
τ_1 (I_1)	0.37	0.34	0.29	0.24	0.18	0.14	0.1	0.05
τ_2 (I_2)	0.75	0.69	0.61	0.51	0.38	0.3	0.21	0.13
τ_3 (I_3)	1.62	1.39	1.24	1.15	1.02	0.93	0.63	0.41

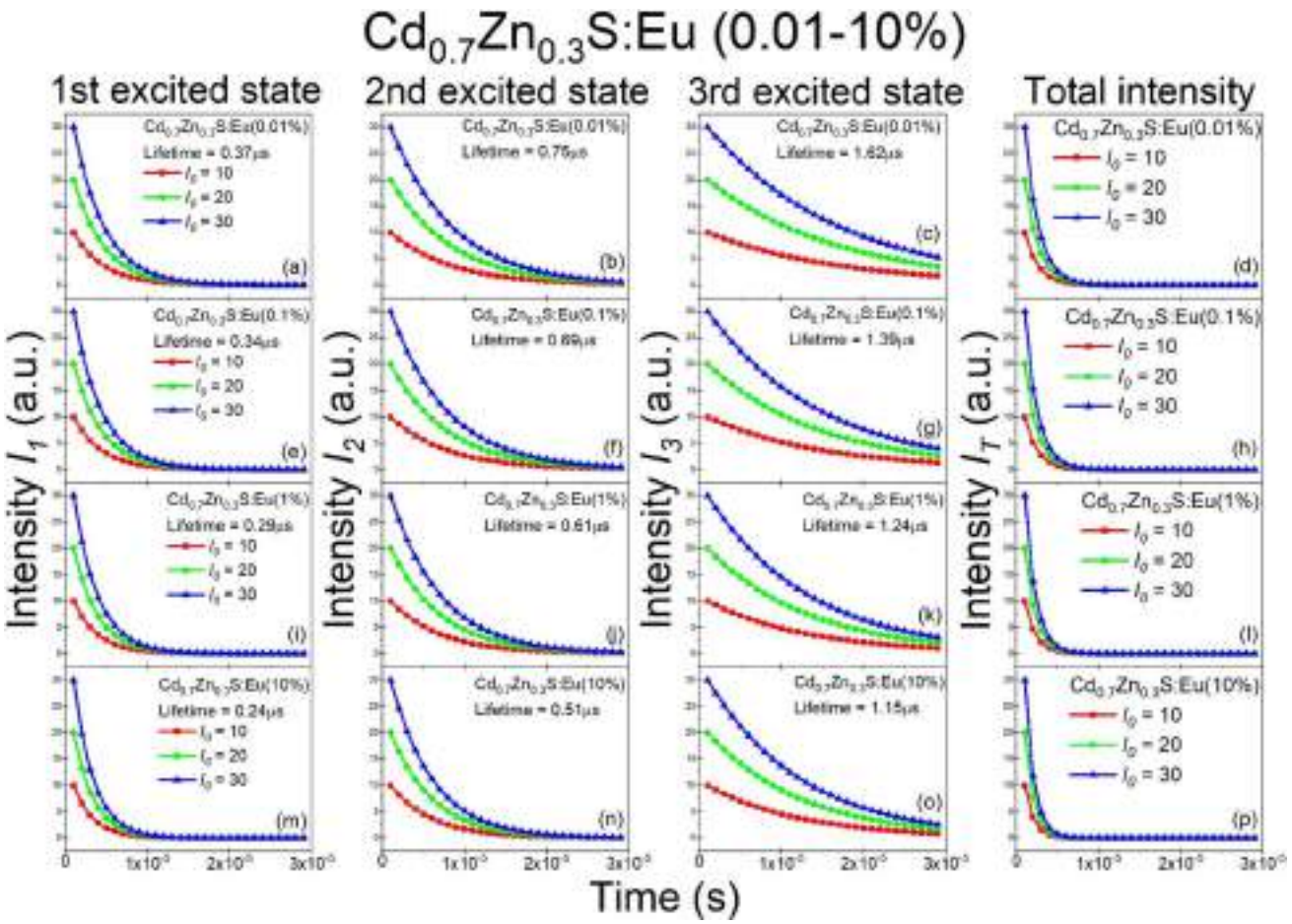

Fig. 4 Simulated time-resolved emission intensity decay curves of $Cd_{0.7}Zn_{0.3}S$:Eu (0.01–10.00%) nanocomposite phosphors

band gap broadening, which quenches emission from deep traps and shallow trap emission becomes dominant, and energy transfer from host to Eu increases with increasing concentration of Zn. The natural logarithm of exponential decay curves is a straight line, while the natural logarithm of hyperbolic decay curves is exponential in nature. From the simulations, it is evident that the parameters of cut-off intensity, individual excited state intensities, and total emission intensity do not cause a change in the shape of the decay curves of the nanophosphors but do cause a shift in the decay curves. However, the trend of the decay curves is dependent on the concentration of the dopant, and the composition of the nanocomposite. The simulated decay curves are able to accurately reproduce the trends of lifetime shortening of the ZnO:Al (0.1–3.0%) and $Cd_{1-x}Zn_xS$:Eu (0.01–10.00%, $x = 0$–0.5) nanophosphors with increasing dopant concentration for all simulated arbitrary cut-off intensities for every individual excited state lifetime exponential. Hence, using these simulations, isolation and clear visualisation of all the individual exponential contributions to the single hyperbolic decay curve is made possible. This will further allow for more reliable and convenient determination of the decay constant 'b' for the distribution of trap sates in the phosphor.

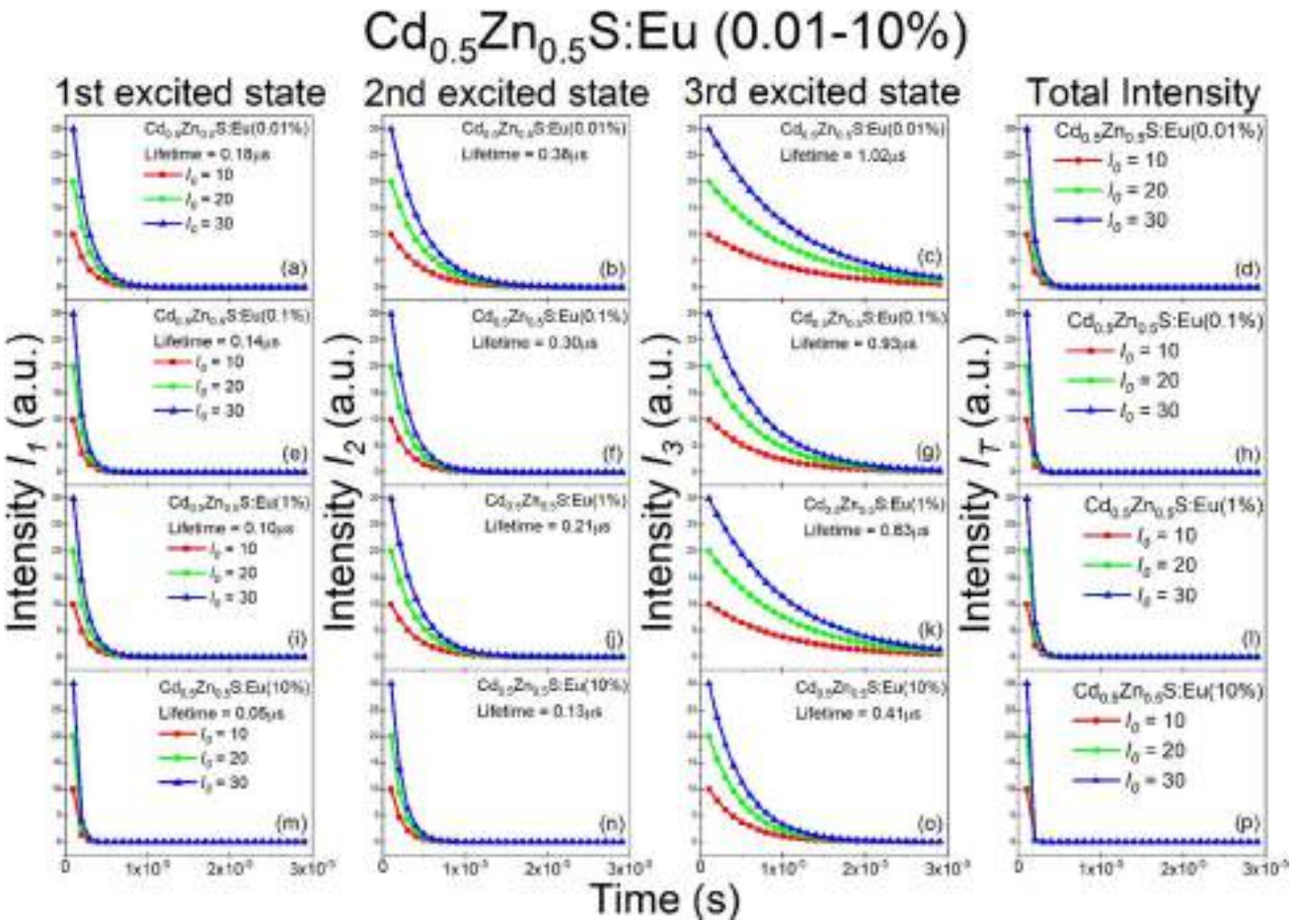

Fig. 5 Simulated time-resolved emission intensity decay curves of $Cd_{0.5}Zn_{0.5}S$:Eu (0.01–10.00%) nanocomposite phosphors

Supplementary Information The online version contains supplementary material available at https://doi.org/10.1007/s00339-023-07055-5.

Acknowledgements S.G. acknowledges the financial support from the Grant Agency of Charles University (GAUK project no. 206423). The author R. K. Choubey acknowledge the financial support from UGC-DAE CSR through a Collaborative Research Scheme (CRS) vide project number CRS/2022-23/1105.

Author contributions All the authors contributed to the present work, conception and design, material preparation, data collection and analysis were performed by the authors. The author's contribution is shown below. The first draft of the manuscript was written by Monika, Reena and Suhaas Gupta. Rest, all the authors helped in analysing the data and commented on the previous version of the manuscript. All the authors read and approved the final manuscript.

Data availability All data generated or analysed during this study have been deposited in this manuscript. All the compared data were properly cited and included in the reference section following the journal style. Also, the data will be available from the corresponding author on reasonable request.

Declarations

Conflict of interest In this manuscript, there is no conflict of interest. I hereby confirm that, the work described has not been published before; it is not under consideration for publication anywhere else; and publication has been approved by all co-authors of this manuscript.

Research data policy and data availability statements All data generated or analysed during this study have been deposited in this manuscript. All the compared data were properly cited and included in the reference section following the journal style. Also, the data will be available from the corresponding author on reasonable request.

References

1. A. Mondal, S. Das, J. Manam, Investigation on spectroscopic properties and temperature dependent photoluminescence of NIR emitting Cr3+ doped zinc gallate long persistent nanophosphor. Physica B **569**, 20–30 (2019)
2. S. Singh, D. Singh, Synthesis and spectroscopic investigations of trivalent europium-doped M2SiO5 (M = Y and Gd) nanophosphor

for display applications. J. Mater. Sci.: Mater. Electron. **31**, 5165–5175 (2020)
3. R. Fouad, M. Saif, Synthesis, spectroscopic and photoluminescence studies of novel Eu3+ nanophosphor complex as fluorescent sensor for highly sensitive detection of latent fingerprints and anti-counterfeiting. J. Mol. Struct. **1217**, 128472 (2020)
4. A. Hooda, S.P. Khatkar, S. Devi, V.B. Taxak, Structural and spectroscopic analysis of green glowing down-converted BYO: Er3+ nanophosphors for pc-WLEDs. Ceram. Int. **47**(18), 25602–25613 (2021)
5. P. Deshmukh, R.K. Deo, A. Ahlawat, A.A. Khan, R. Singh, A.K. Karnal, S. Satapathy, Spectroscopic investigation of upconversion and downshifting properties LaF3: Tb3+, Yb3+: a dual mode green emitter nanophosphor. J. Alloy. Compd. **859**, 157857 (2021)
6. S.S. Nanda, P. Nayak, S.K. Gupta, N.S. Rawat, U.K. Goutam, S. Dash, Structural, optical spectroscopy and energy transfer features of Tb 3+-activated (Y, Gd) F 3 nanophosphors for UV-based LEDs. New J. Chem. **46**(32), 15617–15627 (2022)
7. I. Gupta, D. Singh, S. Singh, P. Kumar, S. Bhagwan, V. Kumar, Phase recognition and spectroscopic characteristics of single-phase Tb3+ doped $Gd4Al_2O_9$ nanophosphors for NUV energized advanced photonic appliances. J. Lumin. **252**, 119327 (2022)
8. I. Gupta, D. Singh, S. Singh, P. Kumar, S. Bhagwan, V. Kumar, Study of structural and spectroscopic characteristics of novel color tunable yellowish-white Dy3+ doped $Gd4Al_2O_9$ nanophosphors for NUV-based WLEDs. J. Mol. Struct. **1272**, 134199 (2023)
9. K. Pratibha, S. Gaurav, S. Shankar, A.K. Dikshit, Y. Dwivedi, Investigations on spectroscopic and optothermal ability of bright red-emitting Cr doped $LiAlSi_3O_8$ nanophosphor. Optik **273**, 170390 (2023)
10. S. Gupta, R.K. Choubey, L.K. Sharma, M.P. Ghosh, M. Kar, S. Mukherjee, Exploring the magnetic ground state of vanadium doped zinc sulphide. Semicond. Sci. Technol. **34**(10), 105006 (2019)
11. S. Tomar, S. Gupta, S. Mukherjee, A. Singh, S. Kumar, R.K. Choubey, Manganese-doped ZnS QDs: an investigation into the optimal amount of doping. Semiconductors **54**, 1450–1458 (2020)
12. S. Tomar, S. Gupta, S. Mukherjee, A. Singh, S. Kumar, V. Kumar, R.K. Choubey, Optical properties of Silica capped Mn doped ZnS quantum dots. Phys. Scr. **96**(6), 065802 (2021)
13. S. Tomar, S. Gupta, A. Priyam, B. Bhushan, A. Singh, U.K. Dwivedi, R.K. Choubey, Temporal evolution of optical absorption and emission spectra of thiol capped CdTe quantum dots. Appl. Phys. A **128**(10), 944 (2022)
14. S. Kumar, A. Jain, S. Panwar, I. Sharma, S. Gupta, M. Dopita, R.K. Choubey, Antibacterial studies of ZnO and silica capped manganese doped zinc sulphide nanostructures. Appl. Phys. A **129**(3), 169 (2023)
15. S. Gupta, A. Kumar, S. Mukherjee, K.K. Kushwah, S.K. Mahobia, P. Patharia, A. Kushwaha, D. Yadav, U.K. Dwivedi, S. Kumar, R.K. Choubey, Temperature-dependent study of the fabricated ZnS/p-Si heterojunction. Physica B Conden. Matter **657**, 414831 (2023)
16. V. Kumar, K. Kumar, H.C. Jeon, T.W. Kang, D. Lee, S. Kumar, Effect of Cu-doping on the photoluminescence and photoconductivity of template synthesized CdS nanowires. J. Phys. Chem. Solids **124**, 1–6 (2019)
17. M. Singhal, J.K. Sharma, H.C. Jeon, T.W. Kang, S. Kumar, Synthesis and characterisation of functional manganese doped ZnS quantum dots for bio-imaging application. Adv. Appl. Ceram. **118**(6), 321–328 (2019)
18. A. Kumar, M. Kumar, V. Bhatt, D. Kim, S. Mukherjee, J.H. Yun, R.K. Choubey, ZnS microspheres-based photoconductor for UV light-sensing applications. Chem. Phys. Lett. **763**, 138162 (2021)
19. S. Kumar, S. Taneja, S. Banyal, M. Singhal, V. Kumar, S. Sahare, S.L. Lee, R.K. Choubey, Bio-synthesised silver nanoparticle-conjugated l-cysteine ceiled Mn: ZnS quantum dots for eco-friendly biosensor and antimicrobial applications. J. Electron. Mater. **50**, 3986–3995 (2021)
20. A. Kumar, M. Kumar, V. Bhatt, S. Mukherjee, S. Kumar, H. Sharma, M.K. Yadav, S. Tomar, J.H. Yun, R.K. Choubey, Highly responsive and low-cost ultraviolet sensor based on ZnS/p-Si heterojunction grown by chemical bath deposition. Sens. Actu. A **331**, 112988 (2021)
21. M. Baradaran, F.E. Ghodsi, C. Bittencourt, E. Llobet, The role of Al concentration on improving the photocatalytic performance of nanostructured ZnO/ZnO: Al/ZnO multilayer thin films. J. Alloy. Compd. **788**, 289–301 (2019)
22. K.H. Abass, M.K. Mohammed, Fabrication of ZnO: Al/Si solar cell and enhancement its efficiency via al-doping. Nano Biomed. Eng. (2019). https://doi.org/10.5101/nbe.v11i2.p170-177
23. S. Liu, G. Li, M. Lan, M. Zhu, K. Miyazaki, Q. Wang, Role of intrinsic defects on thermoelectric properties of ZnO: Al films. Ceram. Int. **47**(12), 17760–17767 (2021)
24. P. Kumar, K.M. Sandeep, V.S. Kindalkar, A. Kote, S.M. Dharmaprakash, Non-polar a-plane oriented ZnO: Al thin films for optoelectronic applications. Physica B **606**, 412721 (2021)
25. L. Dejam, S. Kulesza, J. Sabbaghzadeh, A. Ghaderi, S. Solaymani, S. Ṭalu, M. Bramowicz, M. Amouamouha, A. Hossein Sari, ZnO, Cu-doped ZnO, Al-doped ZnO and Cu-Al doped ZnO thin films: advanced micro-morphology, crystalline structures and optical properties. Results Phys. **44**, 106209 (2023)
26. A. Khan, M. Shkir, M.A. Manthrammel, V. Ganesh, I.S. Yahia, M. Ahmed, A.M. El-Toni, A. Aldalbahi, H. Ghaithan, S. AlFaify, Effect of Gd doping on structural, optical properties, photoluminescence and electrical characteristics of CdS nanoparticles for optoelectronics. Ceram. Int. **45**(8), 10133–10141 (2019)
27. G. Sreedevi, K. Srinivas, M. Subbarao, S. Cole, Investigation on structural and optical properties of CuO doped CdS-Zn3 (PO4) 2 nanocomposite for optoelectronic devices. J. Mol. Struct. **1222**, 128903 (2020)
28. D. Wang, H. Zeng, X. Xiong, M.F. Wu, M. Xia, M. Xie, J.P. Zou, S.L. Luo, Highly efficient charge transfer in CdS-covalent organic framework nanocomposites for stable photocatalytic hydrogen evolution under visible light. Sci. Bull. **65**(2), 113–122 (2020)
29. A. Ghosh, S. Karmakar, F.A. Rahimi, R.S. Roy, S. Nath, U.K. Gautam, T.K. Maji, Confinement matters: stabilization of CdS nanoparticles inside a postmodified MOF toward photocatalytic hydrogen evolution. ACS Appl. Mater. Interfaces. **14**(22), 25220–25231 (2022)
30. M.H. Sun, M.Y. Qi, Z.R. Tang, Y.J. Xu, Dual cocatalysts decorated CdS nanoparticles for efficient dehydrocoupling of thiols into disulfides. Appl. Catal. B **321**, 122019 (2023)
31. C.K. Sagar, P. Sajan, M.J. Bushiri, Eu 3+ and Cu 2+ ions doped ZnS microspheres emission in the yellow–orange region. J. Mater. Sci.: Mater. Electron. **30**, 18220–18226 (2019)
32. C.A. Tuan, V.H. Yen, K.C. Cuong, N.T.M. Thuy, P.M. An, N.T.B. Ngoc, D.T. Hue, A. Xayyadeth, Y. Peng, N.N. Le, N.T.K. Van, N.T. Kien, C.V. Ha, Optical properties and energy transfer mechanism of Eu3+, Ce3+ doped and co-doped ZnS quantum dots. J. Lumin. **236**, 118106 (2021)
33. B. Poornaprakash, S.P. Vattikuti, K. Subramanyam, R. Cheruku, K.C. Devarayapalli, Y.L. Kim, V.R.M. Reddy, H. Park, M.S.P. Reddy, Photoluminescence and hydrogen evolution properties of ZnS: Eu quantum dots. Ceram. Int. **47**(20), 28976–28984 (2021)

34. V. Lahariya, S.J. Dhoble, Development and advancement of undoped and doped zinc sulfide for phosphor application. Displays **74**, 102186 (2022)
35. U. Latief, S.U. Islam, Z. Khan, M.S. Khan, Luminescent Manganese/Europium doped ZnS quantum dots: tunable emission and their application as fluorescent sensor. J. Alloy. Compd. **910**, 164889 (2022)
36. M. Maiberg, R. Scheer, Theoretical study of time-resolved luminescence in semiconductors. I. Decay from the steady state. J. Appl. Phys. **116**(12), 123710 (2014)
37. M. Maiberg, R. Scheer, Theoretical study of time-resolved luminescence in semiconductors. II. Pulsed excitation. J. Appl. Phys. **116**(12), 123711 (2014)
38. M. Maiberg, T. Hölscher, S. Zahedi-Azad, R. Scheer, Theoretical study of time-resolved luminescence in semiconductors. III. Trap states in the band gap. J. Appl. Phys. **118**(10), 105701 (2015)
39. K. Singh, S. Kumar, N.K. Verma, H.S. Bhatti, Photoluminescence properties of Eu 3+-doped Cd 1–x Zn x S quantum dots. J. Nanopart. Res. **11**, 1017–1021 (2009)
40. D. Kumar, S. Kumar, H.S. Bhatti, Laser-Induced photoluminescent studies of Al-doped zinc oxide nanoparticles. Int. J. Nanosci. **9**(05), 439–445 (2010)